




## Article

# A Computer Model of a Marx Generator Charging a Coaxial Switched Wave Oscillator

Bartosz Chaber , Wiktor Łodyga  and Jacek Starzyński 

Faculty of Electrical Engineering, Warsaw University of Technology, 00-661 Warsaw, Poland

\* Correspondence: bartosz.chaber@pw.edu.pl

**Abstract:** The paper describes an axisymmetric Finite-Difference Time-Domain computer model of a coaxial Switched Wave Oscillator integrated with a dipole antenna. The model analyzes the operation of a realistic circuit model of a multistage Marx generator that charges the oscillator to a high voltage. The initial field distribution is calculated with an electrostatic finite-difference method solver to speed up the time-domain analysis. The work presents the results of our circuit model of a Marx generator's simulations of the charging phase, followed by the results from the discharge phase, using our axisymmetric Finite-Difference Time-Domain model. Our work describes new and fast numerical solvers that can observe the operation of Switched Wave Oscillator systems (also considering the connected antenna). The codes could be used in the process of designing such a system. Advanced boundary conditions modeling the spark gap and oscillator's excitation set our work apart from the other attempts in the literature.

**Keywords:** FDTD; PML; switched wave oscillators



**Citation:** Chaber, B.; Łodyga, W.; Starzyński, J. A Computer Model of a Marx Generator Charging a Coaxial Switched Wave Oscillator. *Energies* **2024**, *17*, 4644. <https://doi.org/10.3390/en17184644>

Academic Editors: Adrian Ilinca and Ahmed F. Zobaa

Received: 5 July 2024

Revised: 19 August 2024

Accepted: 13 September 2024

Published: 17 September 2024



**Copyright:** © 2024 by the authors. Licensee MDPI, Basel, Switzerland. This article is an open access article distributed under the terms and conditions of the Creative Commons Attribution (CC BY) license (<https://creativecommons.org/licenses/by/4.0/>).

## 1. Introduction

Systems that generate strong pulses of electromagnetic fields have extremely wide applications, from Nuclear Electromagnetic Pulse (NEMP) simulators for the electromagnetic compatibility testing of military equipment, to radiating systems for disrupting electronic devices, to systems for disinfection, or research on the electroporation of cell membranes. Such systems consist most often of a high-voltage DC power supply, a generator that produces an electromagnetic pulse, and an element responsible for its effective radiation. All these components are non-trivial to develop due to the need to ensure very high breakdown strength and simultaneously maintain small insulation gaps to increase capacitance. Moreover, the power supply (as an electronic device) is sometimes easily disturbed by the close, strong electromagnetic field generated by the pulsed system.

Switched Wave Oscillators (SWOs) have been studied for more than 20 years as elements that form a high-voltage pulse and enable its efficient radiation [1]. In its simplest form, an SWO is a coaxial long line with low characteristic impedance that is charged to a high voltage (e.g., by a voltage multiplier). One end is connected to the antenna, while the other end is short-circuited by a spark gap, which causes propagation and multiple reflections of the pulse inside the coaxial line. A review paper [2] presents other variants of the oscillator, while a currently interesting circuit is a variant with a long line attached, open at one end, presented in [3]. A similar variant is presented in [4], where a prototype system with a horn antenna excited by a transverse-electromagnetic wave is described. In [5], a helical antenna is connected to the output of an oscillator as an example of a directional antenna.

Among the mentioned works, the design process of the oscillator is mainly supported by circuit simulations [3,5]. Simulations based on electromagnetic wave propagation models are used in [6,7], while simulations of the electrostatic field before the spark gap was shorted are used in [4]. Some recent works on coaxial SWOs employ 3D simulations

in CST Microwave Studio, where the spark-gap switch is modeled often as a voltage source [8,9]. While there are papers covering simulations of coaxial SWOs with an antenna in the frequency domain [10], we have not found a time-domain analysis with a realistic switch model. The authors of [11] describe a 3D computer simulation in CST Microwave Studio of a parallel-plate transmission line SWO, where the spark gap is modeled as a low-impedance port. To the best of our knowledge, no model integrating a realistic circuit model of a Marx generator, a time-domain model of a coaxial Switched Wave Oscillator, and an antenna has been presented.

The main contribution of our research work is a numerical solver for the time-domain simulation of a Switched Wave Oscillator with a realistic dipole antenna and a time-varying impedance acting as a spark-gap switch. The solver is able to analyze the transient effects of the charging and discharging of the electromagnetic pulse generation system.

## 2. Axisymmetric Electromagnetic Field Solver

Solving Maxwell's equations in the time domain is a demanding task. One of the most efficient methods in computational electromagnetics is Finite-Difference Time Domain (FDTD), which is a widely known and popular method due to its versatility, ease of implementation, and potential for parallelization. The main strength of FDTD is its explicit update scheme that enables calculating electric and magnetic fields without the need to solve large systems of linear equations. Tied to this advantage is also a drawback: the constraint for the time step for stable simulations is rather strict [12].

To partially alleviate that, we have built our solver in such a manner that each time step is calculated fast, without additional memory allocations or unnecessary branching. This way, although the number of time steps is large, the computational cost is low. By default, we use the maximum allowed time step:

$$\Delta t = \min(\Delta z, \Delta r) / c\sqrt{2},$$

where  $c$  is the speed of light in the vacuum, and  $\min(\Delta z, \Delta r)$  selects the smaller spatial step: either along  $z$ - or  $r$ -direction. When the maximum propagation speed is smaller than the speed of light (i.e., we consider only waves propagating in some dielectric), the default time step would be too fine, and we can make it larger.

Our FDTD solver has been compared to two commercial packages in terms of accuracy and computational cost in [13], and it outperformed them in a number of unknowns updated in a unit of time. In this paper, we will describe its inner workings in greater detail, with a focus on how it enables simulating SWOs. Part of the achieved performance is due to the static generation of the code of each simulation. The function for computing a single time step is generated based on the boundary conditions that are prescribed. It enables precomputing the indices for which boundary conditions are applied.

One of the most widely used schemes for FDTD is the Yee scheme, where we solve for both electric and magnetic field components located at different locations of a regular computational grid (see Figure 1). In our simulator, we distinguish axial electric field component  $E_z$  from radial electric field  $E_r$ . The two fields are located in the middle of either edge parallel to the axis of symmetry ( $r = 0$ ) or perpendicular to the axis. For each edge, we can define a separate boundary condition that is applied to it. By default, the fields at all boundary edges are assigned a zero value, which corresponds to a Perfect Electric Conductor (PEC). We can override it by applying additional boundary conditions, i.e., Perfect Magnetic Conductor (PMC) or Surface Impedance Boundary Condition (SIBC). Axial edges on the axis of symmetry are automatically applied via Perfect Magnetic Conductor to maintain the symmetry of the solution [14]. For edges that have no prescribed boundary

condition, their values are updated according to the discretized Maxwell equations using adjacent field locations:

$$H_{\theta}|_{i,j}^{n+1/2} = H_{\theta}|_{i,j}^{n-1/2} + \frac{\Delta t}{\mu_0} \frac{E_z|_{i,j+1}^n - E_z|_{i,j}^n}{\Delta r} - \frac{\Delta t}{\mu_0} \frac{E_r|_{i+1,j}^n - E_r|_{i,j}^n}{\Delta z}, \quad (1)$$

$$E_z|_{i,j}^{n+1} = \frac{1-\gamma}{1+\gamma} E_z|_{i,j}^n + \frac{\Delta t}{\varepsilon} \frac{H_{\theta}|_{i,j}^{n+1/2} - H_{\theta}|_{i,j-1}^{n+1/2}}{2r|_{i,j}} + \frac{\Delta t}{\varepsilon} \frac{H_{\theta}|_{i,j}^{n+1/2} - H_{\theta}|_{i,j-1}^{n+1/2}}{\Delta r}, \quad (2)$$

$$E_r|_{i,j}^{n+1} = \frac{1-\gamma}{1+\gamma} E_r|_{i,j}^n - \frac{\Delta t}{\varepsilon} \frac{H_{\theta}|_{i,j}^{n+1/2} - H_{\theta}|_{i-1,j}^{n+1/2}}{\Delta z}, \quad (3)$$

where  $H_{\theta}|_{i,j}^{n+1/2}$  is the out-of-plane oriented magnetic field component, defined for  $t = (n + 1/2)\Delta t$ , in the center of the cell  $i, j$ ,  $E_z|_{i,j}^n$  is the axial electric field component associated with edge  $i, j$  at time  $t = n\Delta t$ ,  $E_r|_{i,j}^n$  is the radial electric field component defined at edge  $i, j$  at time  $t = n\Delta t$ , and  $\gamma = \sigma \frac{\Delta t}{2\varepsilon}$  is the loss coefficient. The uniform grid with  $N, M$  grid nodes defines  $(N - 1), (M - 1)$  rectangular cells (with width of  $\Delta z$  and height of  $\Delta r$ ). Each node has its axial and radial coordinates  $(z_{i,j}, r_{i,j})$ . A cell  $i, j$  has four edges: two axial,  $(i, j)$  and  $(i + 1, j)$ , and two radial,  $(i, j)$  and  $(i, j + 1)$ . Equations (1)–(3) assume that the edges and cells are defined for the same material with permittivity  $\varepsilon$ , permeability  $\mu = \mu_0$ , and conductivity  $\sigma$ .

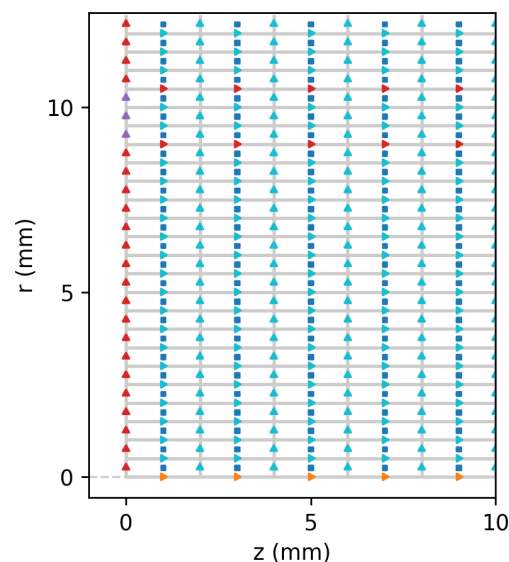


**Figure 1.** (Color version online) Yee grid for an axisymmetric domain ZR. Triangles mark locations at which the electric field is stored. Square marks are the locations of out-of-plane magnetic field. Red triangles mean PEC, orange triangles mean PMC, while purple ones mean SIBC. Blue triangles mean edges without a prescribed boundary condition.

To support multiple dielectric materials, there is also a dielectric interface condition that is automatically marked at edges shared by different materials. According to [15], the material interface might be placed at arbitrary distance between nodes of Yee grid. In our solution, we assume that the boundary interfaces are located directly at edges of the computational grid. It effectively means that, if the real boundary is not resolved by the grid, the dielectric interface will be shifted no more than half the grid step.

Truncating the computational domain requires special handling of boundaries that should absorb electromagnetic waves simulating an open boundary and prevent artificial reflections from the domain's boundary. Our solver supports both a special boundary, called Surface Impedance Boundary Condition (implemented according to [16]), and a special material called Perfectly Matched Layer (PML, implemented according to [17]). Sur-

face Impedance Boundary Condition is a boundary with a prescribed wave impedance  $\eta = E_t/H_t$  where  $E_t$  and  $H_t$  are electric or magnetic components, tangential to the boundary with SIBC. In our code, we made the wave impedance time-dependent to model closing of a spark-gap switch, similar to the time-varying resistor in [18].

As the FDTD model is axisymmetric, the number of unknown field values is much lower than in the 3D case. On the other hand, only electromagnetic field modes and geometries that exhibit the rotational symmetry can be represented by  $E_z$ ,  $E_r$ , and  $H_\theta$ . The model assumes that  $E_\theta = 0$  V/m and  $H_z = H_r = 0$  A/m. The presented implementation of FDTD has been kept simple, so it does not implement any conformal grid elements. This means that all curved surfaces have to be discretized using a staircase approximation. The main technical challenge of the presented numerical solver was to avoid the cost of solving the steady-state electric field distribution after charging of an SWO. We have resolved this by writing an FDTD-compatible finite-difference electrostatic solver that is presented in Section 4.

### 3. Realistic Circuit Model of a Marx Generator

In order to work properly, Switched Wave Oscillators have to be charged with a high voltage. One of the popular choices of such a high voltage source is a Marx generator as it is relatively inexpensive and simple to build. However, Marx generators do not provide a DC voltage but a pulse similar to one described by a double-exponential function:

$$U(t) = A \exp(-\alpha t) - A \exp(-\beta t),$$

where  $U(t)$  is the voltage at time  $t$ , and  $\alpha$  and  $\beta$  are coefficients with units of Hz defining the rise time and the fall time of the pulse.  $A$  is the maximum amplitude of the voltage pulse.

The shape of the pulse plays a crucial role as it can affect the proper operation of an SWO. A pulse that is too fast can cause SWO to breakdown too early, when the oscillator is still not fully charged. However, the accurate approximation of the Marx generation pulse shape is not a trivial task, mainly because of the fact that multistage Marx generator utilizes many spark gaps, which are strongly nonlinear. Moreover, the spark-gap breakdown characteristic depends on multiple other measures, such as the type of gas in which it is immersed, the gas density, electrodes' distance, electrodes' material, a transient characteristic of a voltage applied between electrodes, or the presence of some ionizing radiation (e.g., due to a discharge flare in an adjacent spark gap). Even when all these are known, the spark-gap breakdown is still a stochastic process, which is very challenging to simulate accurately.

Currently one of the most advanced circuit models of a spark gap is the one described in [19] by Pouncey and Lehr. Based on their work, developed in LTSpice, we have created our own solution, which utilizes an open-source nonlinear circuit solver ACME.jl [20]. In this approach, the spark gap is represented by a nonlinear RL circuit element with parallel capacitor representing capacitance between electrodes. The main parameters of the circuit are gas pressure, electrode distance, and capacitance between electrodes. The model utilizes multiple experimentally determined formulas for static breakdown voltage, breakdown delay, channel resistance, channel radius, and channel inductance (derived from channel radius). These formulas can be adjusted or replaced to better fit the model to the problem being solved. The flowchart of the model's algorithm is presented in Figure 2. The algorithm is executed in every time step of a circuit simulation.

To predict the voltage applied to an SWO, we utilized the described spark-gap model coupled with a circuit model of a three-stage Marx generator (described later in Section 5.1). Because of the fact that Marx generator circuit rapidly becomes very complex with increasing number of stages, we created a tool to accurately generate such circuits. Our paper covering the topic of a realistic spark gap and Marx generator in ACME.jl is currently under review (pending publication). The resulting circuit simulation incorporates multiple spark-gap models to calculate realistic output voltage pulses applied to a capacitive load (see Figure 3).

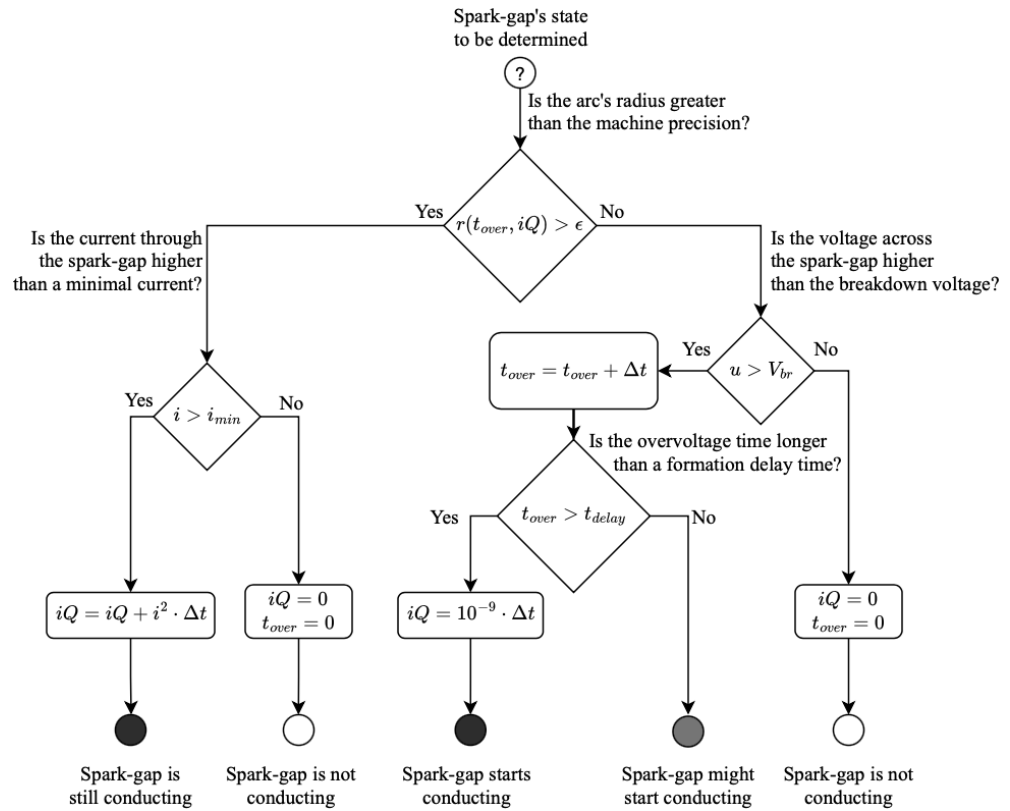


**Figure 2.** Flowchart of the spark-gap model algorithm ( $u$ ,  $i$ —spark-gap voltage and current;  $r$ —channel radius;  $\epsilon$ —machine precision;  $V_{br}$ —breakdown voltage;  $iQ$  value of an integral used to calculate channel resistance;  $t_{delay}$ —time required for channel to develop;  $t_{over}$ —time of spark-gap overvoltage;  $\Delta t$ —time step).

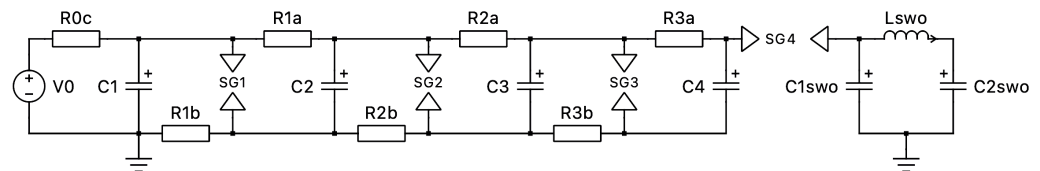


**Figure 3.** Circuit model of a three-stage Marx generator connected to a transmission line in the form of a single  $\pi$ -stage.

#### 4. Electrostatic Initial Conditions

Simulation of charging a Switched Wave Oscillator is interesting in the context of some transient effects, but, when the capacitance of the oscillator is large and the grid resolution fine enough, it might take many time steps to reach a steady state. A natural solution for this problem is solving an electrostatic problem and transferring its solution as some initial values to the transient simulation. Finite-Difference Method (FDM) is an effective method to solve Laplace’s equation for electric potential  $\phi$ . Conveniently, FDM might share the grid with FDTD for transferring just the electric fields between the electrostatic and electromagnetic solvers.

In our electrostatic simulation, all PMLs are neglected and substituted with their base materials, and SIBC and PMC are replaced with Neumann Boundary Conditions (for which  $\partial\phi/\partial\hat{n} = 0$ ). A prescribed electric potential can be assigned to nodes of a Yee grid, representing the situation when the inner conductor of an SWO is charged. Currently, we solve the electrostatic problem by assembling a system of linear equations, taking into account different material properties of dielectrics, as presented in [21].

When the electric potential  $\phi$  is found in the nodes of the grid, electric field can be computed with finite differences at the centers of each edge. This scheme is of course

compatible with our FDTD solver. If we assume that, after the SWO is fully charged, there should be no currents flowing, the magnetic field is, therefore, approximately zero.

## 5. Computer Simulations

Our test case will be a coaxial Switched Wave Oscillator. The inner conductor is elongated in the form of a dipole antenna matched approximately to the frequency generated by the SWO. The computer simulations cover both a charging phase and a discharging phase, where we observe an electromagnetic pulse radiated by an antenna.

The outer radius of the oscillator's dielectric is  $R_o = 10.4$  mm, the inner radius is  $R_i = 9$  mm, and the relative permittivity of the dielectric is  $\epsilon_r = 4.0$  (material is FR4). The parameters result in the characteristic impedance of  $Z = 4.33 \Omega$ . The transmission line is  $L = 248$  mm long, which, according to [3], corresponds to the transit time of  $\tau = 1.65$  ns and the base frequency of oscillations  $f = 151.1$  MHz. The antenna is a dipole antenna, with a single arm of  $L_a = 415$  mm, which is tuned to a slightly larger frequency  $f_c = 172$  MHz. We simulate a computational domain that extends to 1.2 m in  $z$ -direction and 0.2 m in  $r$ -direction. The grid is discretized with 601 nodes in  $z$ -direction ( $\Delta z = 2$  mm) and 401 nodes in  $r$ -direction ( $\Delta r = 0.5$  mm).

### 5.1. Charging Simulation

Simulations of transient effects during charging of the oscillator-antenna system are presented in two phases. In the first one, a circuit model of a three-stage Marx generator is carried out, with SWO represented as a single  $\pi$ -section of a transmission line. The single section consists of an inductor  $L_{SWO} = 7.23$  nH and two capacitances in parallel that sum to the total capacitance of the SWO  $C_{SWO} = 192$  pF + 192 pF = 384 pF.

The Marx generator is charged with a DC voltage  $V_0 = 5$  kV, connected with a 2 M $\Omega$  resistor. Each stage consists of two charging resistors (1 M $\Omega$  each), capacitor  $C = 2$  nF, and a spark gap. The three spark gaps differ in their inter-electrode distances (1.2 mm, 1.4 mm, and 1.65 mm) to accommodate higher voltages at each stage of the generator. The last spark gap has the distance between its electrodes  $d = 1.9$  mm. In the circuit simulation, we start with initially charged capacitors and all spark gaps in non-conductive states. The first spark gap is then triggered at the start of the transient state simulation. We monitor voltages at all spark gaps and also at the load. We run the circuit simulation for 200,000 time steps with the time resolution  $\Delta t = 0.2$  ps. The output waveform can be seen in Figure 4.

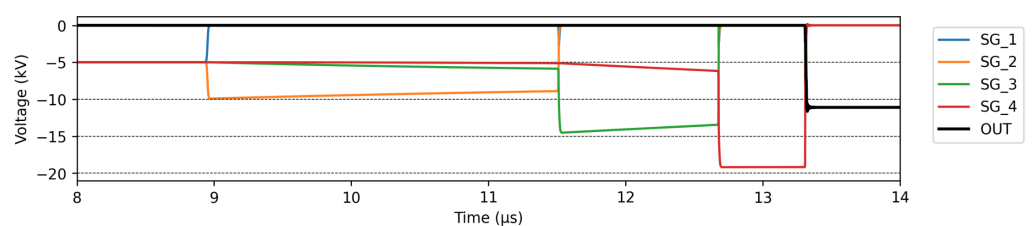


**Figure 4.** Voltage waveforms at the spark gaps ( $SG_1$ ,  $SG_2$ ,  $SG_3$ , and  $SG_4$ ) and at the load of the generator (OUT).

What can be seen in Figure 4 is that the output voltage pulse has a long tail, which corresponds to relatively low values of  $\beta \sim 10^3$ . In the second phase of the charging simulation, the input signal is fed to the SWO as a soft-source of a current density [13]. The current density is in the form of a double-exponential function with the following parameters:  $A = 12$  kV,  $\alpha = 1$  GHz, and  $\beta = 1$  kHz. The time step for FDTD simulation of SWO charging is  $\Delta t = 1.179$  ps; we simulate the charging until  $t = 30$  ns. Two probes registered electric field values at different parts of the computational domain: one ( $E_r$ ) at the base of the dipole antenna, and another ( $E_z$ ) approximately 20 cm in the radial direction from the first probe. The plot of the signals registered by the two probes can be seen in Figure 5. It is noticeable that the oscillator-antenna system is charged almost monotonously to the maximum voltage after 6.5 ns. It takes at least 5500 time steps to converge to the

electrostatic solution. The second interesting effect is a pulse registered 20 cm from the axis of the dipole. Its amplitude is normalized (its actual amplitude is  $1700\times$  smaller than the input signal), but we can clearly see the propagation time of the electromagnetic wave.

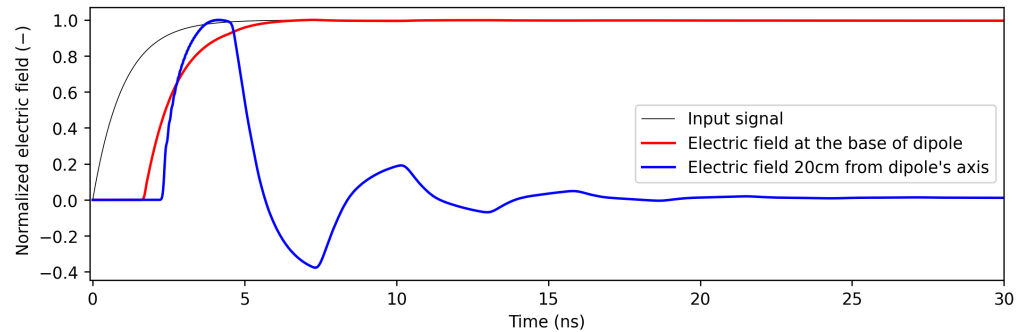


**Figure 5.** Electric fields registered by two probes placed near the base of the dipole antenna and at  $z = 24.8$  cm,  $r = 20$  cm.

### 5.2. Discharge Simulation

The discharge simulation requires a fine time step to capture the details of the collapsing voltage wave. On the other hand, we would like to simulate the charging phase with the largest time step possible. The results in Figure 5 indicate that the system in fact reaches a steady state. In the discharge simulation, we will use our FDM solver to find the electrostatic solution and apply it as initial conditions to the FDTD simulation.

Figure 6a presents the electrostatic solution of the electric potential  $\phi$  defined in the nodes of Yee grid. The electric potential is always solved for 1 V voltage difference, so it can be easily scaled as the initial conditions for the electromagnetic simulation. The large gray box represents a metal reference plane. This way, we simulate the dipole antenna by analyzing its single arm over an approximately infinite ground plane (the nodes of the metal have prescribed  $\phi = 0$ ). The time step of the simulation is the same as for the charging phase. This time, we simulate it until  $t = 140$  ns.

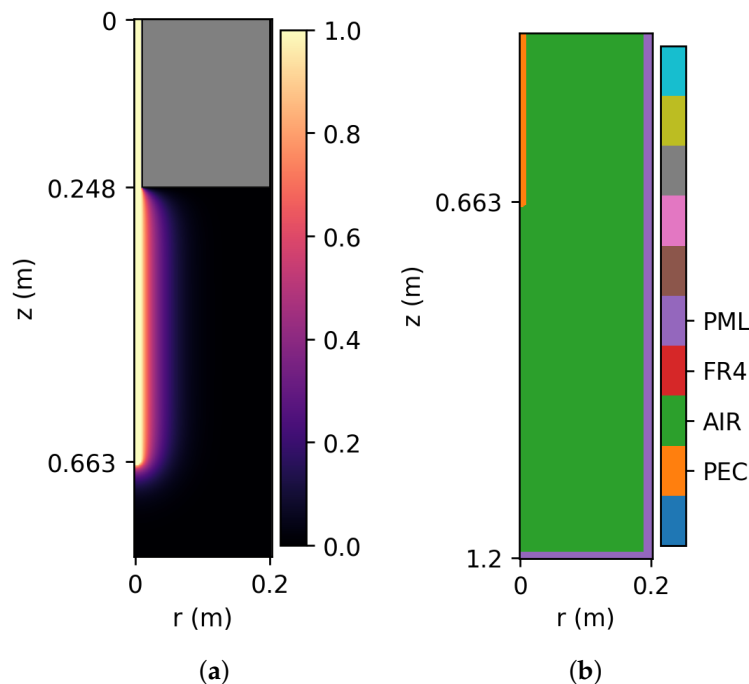


**Figure 6.** (Color version online) Electric potential found with the FDM solver (a) and the overview of materials used in FDTD simulation (b).

To make the computational domain smaller, its outer side and the top layer are filled with a Perfectly Matched Layer with  $\sigma_{\max} = 0.00446$  S/m and the other parameters of air. The PML is 10 mm thick, and its boundaries are backed with Surface Impedance Boundary Conditions acting as an additional absorbing boundary condition. Different materials defined for nodes of Yee grid are presented in Figure 6b (the figure is only a part of the computational domain, so there are no visible nodes marked FR4).

Another Scattering Impedance Boundary Condition has been defined at the input coaxial port of the oscillator. The impedance at this port is time-varying as an S-shaped curve (i.e., generalized logistic function) that smoothly transitions from a high surface impedance ( $\eta = 1$  T $\Omega$ , approximating Perfect Magnetic Conductor) to a low impedance of about 200 m $\Omega$ , representing spark's resistance.

Figure 7 shows both the signal of propagating inside the oscillator (measured at the base of the dipole antenna) and the radiated signal measured at approximately 20 cm from the axis of the antenna. At first, the electric field at the base of the dipole is constant, which confirms that the solution from FDM is compatible with FDTD solver. The high-impedance SIBC acts as an open boundary and "holds" the oscillator charged. Then, at  $t = 27$  ns, the impedance is switched according to the S-shaped curve ( $A = 10^{12}$   $\Omega$ ,  $K = 0.2$   $\Omega$ ,  $C = 1$ ,  $Q = 1$ ,  $B = 3$  GHz, and  $\nu = 1$ ).

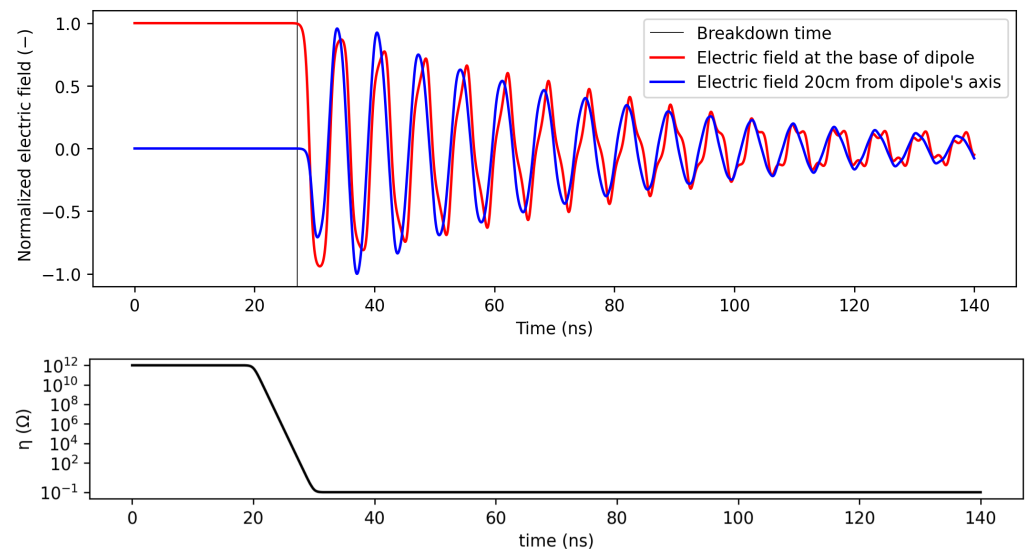


**Figure 7.** Normalized electric field waveforms measured at the dipole's base and at  $z = 24.8$  cm,  $r = 20$  cm (top part of the figure), and the time-varying surface impedance (presented in logarithmic scale) representing a closing spark gap (bottom part of the figure).

## 6. Parametric Analysis

Equipped with a model capable of analyzing the SWO-antenna system, one could determine how some selected design parameters influence the signal radiated by the antenna. We have considered four main parameters, i.e., the antenna length, the spark gap's wave impedance, the length of the transmission line, and the radius at the tip of the antenna. All the parameters affect the waveform registered 20 cm from the antenna base. In the case of the transmission line analysis, the base does move in the  $z$ -direction, along with the probe. The reference model presented in the previous experiments has an antenna length of 415 mm, and the wave impedance at the spark gap  $0.001\eta = 0.001\eta_0\sqrt{\mu_r/\epsilon_r} = 0.001\eta_0\sqrt{1/4} \approx 188$  m $\Omega$ ; assuming that relative permittivity of FR4 is  $\epsilon_r = 4$ , its relative permeability is  $\mu_r = 1$ , and the intrinsic impedance of free space  $\eta_0 \approx 377$   $\Omega$ . The transmission line of the reference model is 248 mm long, and the radius at the tip of the antenna is the same as the radius of the inner conductor of the transmission line (9 mm). In each analysis, only the tested parameter changes, and the rest have the default values of the reference model.



The influence of the length of the arm of the dipole antenna is two-fold. Firstly, the oscillating signal views antennas of different lengths as different loads, so the output signal decays faster or slower than for the reference model (see the top part of Figure 8). Secondly, the tuning of the SWO and the antenna's resonance frequency affect the amplitude of the registered signal (see the bottom part of Figure 8).

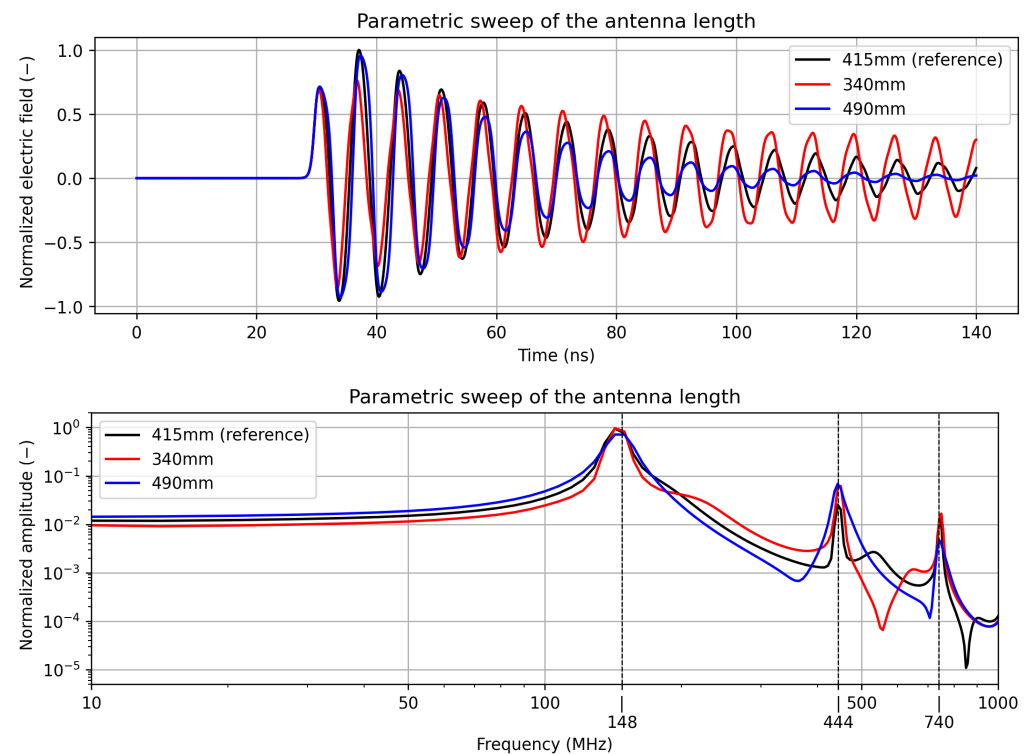


**Figure 8.** (Color version online) Parametric sweep results for different lengths of the dipole antenna are presented in the time domain (**top**) and the frequency domain (**bottom**) for the radiated field. The vertical dashed lines mark the first, third, and fifth fundamental frequencies of the SWO.

The spark gap at the end of the SWO's transmission line is modeled as a time-variant Surface Impedance Boundary Condition, which changes its wave impedance to some final small value that represents a shorted connection. The smaller the final value, the more slowly the signal in the transmission line decays as less power is dissipated in the spark. The decay can be observed both in the time domain and frequency domain in Figure 9.

The length and propagation speed of the transmission line determine the fundamental frequencies of the generated oscillations. The propagation speed is related to the material properties of a given transmission line dielectric. The longer the transmission line, the longer the signal travels in the SWO, leading to lower oscillation frequency. Figure 10 presents the effect of different transmission line lengths in our model. We can clearly see a shift in the fundamental frequencies of the oscillations.

The last parameter being tested is the shape of the antenna. In this test, the radius of the antenna tip is increased (see the left part of Figure 11). Making the end of the arm wider should result in a slight increase in the antenna's bandwidth [22]. The base of the antenna has the same radius as the inner conductor of the transmission line. The radius is then linearly increased to the radius of the antenna's tip. The tip of the antenna is a sphere of the same radius. The time-domain plots (see the right part of Figure 11) suggest an increase in the amplitude as the antenna becomes more conical. We can also observe that the radiated signal decays faster.

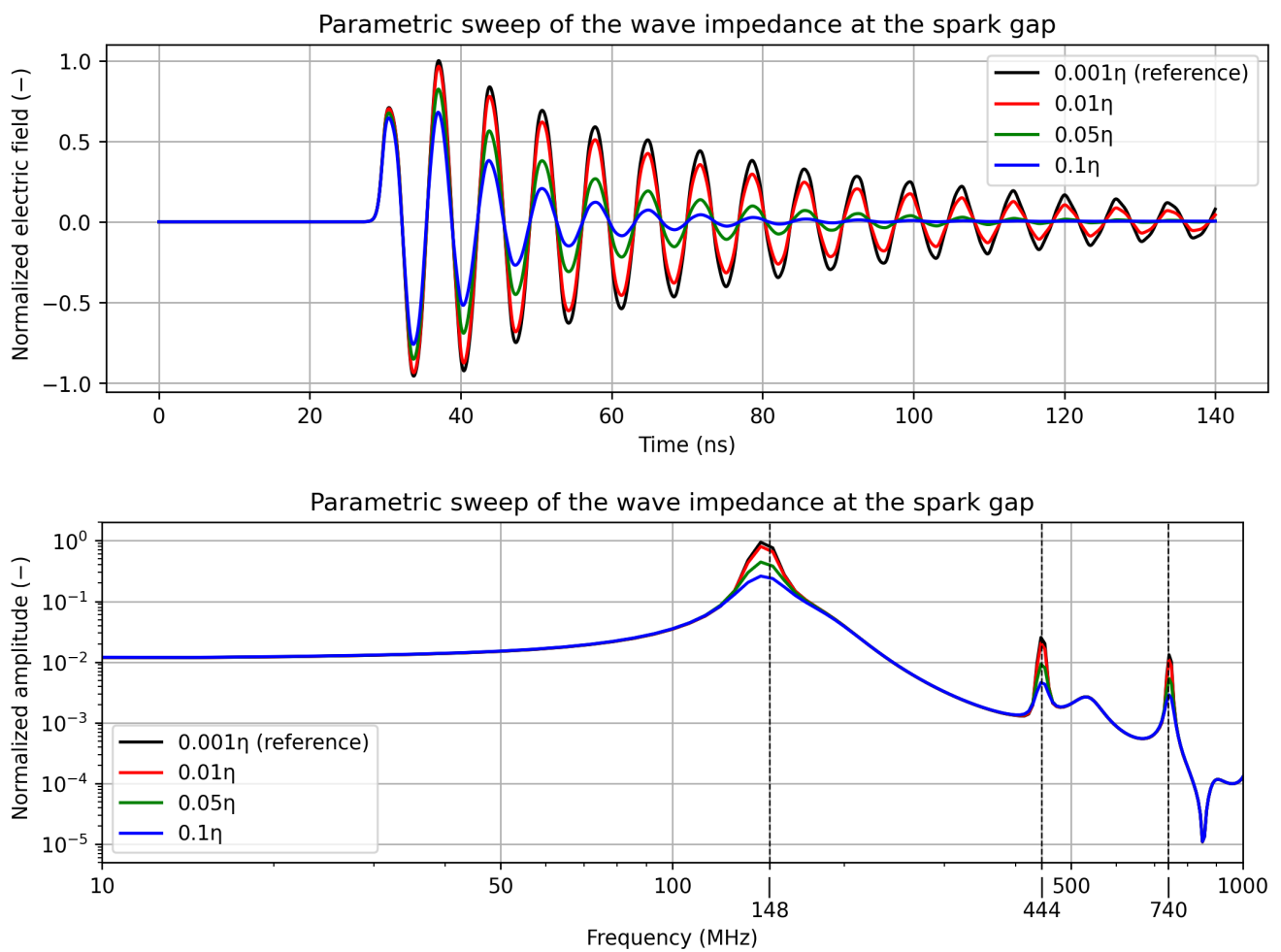


**Figure 9.** (Color version online) Time-domain (top) and frequency-domain (bottom) plots of the output signal measured by the field probe at  $z = 24.8$  cm,  $r = 20$  cm for different impedance values at the spark gap. The vertical dashed lines mark the first, third, and fifth fundamental frequencies of the SWO.

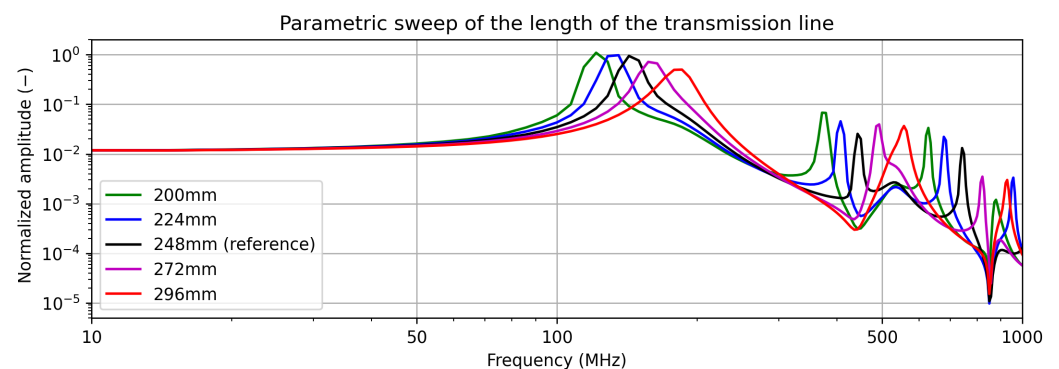


**Figure 10.** (Color version online) The changes in the oscillator's fundamental frequency for different lengths of the transmission line.

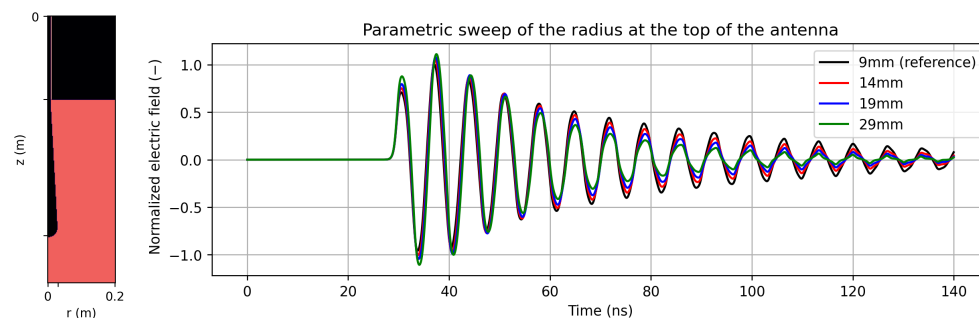


**Figure 11.** (Color version online) The schematic view of the conical antenna shape (**left**), and the results of the parametric sweep for different antenna tip radii (**right**).

This paper covers only the parameters of the electromagnetic part of the model. The analysis of the circuit model will be presented in a separate paper.

## 7. Results

This work describes a computer model of a Switched Wave Oscillator integrated with a dipole antenna. The toolset for modeling the device consists of a few other custom tools: a circuit simulator of a Marx generator (with an advanced spark-gap model), an electrostatic field solver based on the FDM, and an electromagnetic field solver based on the FDTD method.

The tools are tested against an exemplary coaxial Switched Wave Oscillator, simulated through the charging phase, until the discharge and radiation of the generated oscillations.

It has been confirmed that, in most cases, calculating an electrostatic field distribution is a viable alternative to simulating the charging phase with an electromagnetic field solver.

## 8. Future Work

Despite its computational efficiency, the axisymmetric model is quite limiting in terms of the geometries that can be analyzed. We plan to extend the software to make it even more versatile and capable of simulating real designs of Switched Wave Oscillators. Although fast, the FDTD method might have difficulty in correctly representing a geometry with fine details due to its structured grid. In the future, we plan to pursue building an FEM-based SWO simulator that would be fully coupled with the circuit model of spark gaps and Marx generators. Another goal is to build the Marx generator and the coaxial SWO presented in the computer simulations to verify their results with the measurements of the radiated electromagnetic field by the dipole antenna.

**Author Contributions:** Conceptualization, J.S. and B.C.; methodology, B.C.; software, B.C. and W.L.; validation, B.C.; formal analysis, B.C.; investigation, B.C.; resources, J.S.; data curation, B.C.; writing—original draft preparation, B.C.; writing—review and editing, B.C., W.L., and J.S.; visualization, B.C.; supervision, J.S.; project administration, J.S.; funding acquisition, J.S. All authors have read and agreed to the published version of the manuscript.

**Funding:** This research was funded by the internal project granted by the Warsaw University of Technology.

**Data Availability Statement:** The original contributions presented in the study are included in the article, further inquiries can be directed to the corresponding author.

**Conflicts of Interest:** The authors declare no conflicts of interest.

## References

1. Baum, C.E. Circuit and Electromagnetic System Design Notes 45: Switched Oscillators. 2000. Available online: <https://ece-research.unm.edu/summa/notes/CESDN/CESDN45.pdf> (accessed on 1 May 2024).
2. Baum, C.E. Variations on the switched-oscillator theme. In Proceedings of the 2010 URSI International Symposium on Electromagnetic Theory, Berlin, Germany, 16–19 August 2010. [CrossRef]

3. Ryu, J.; Yu, J.W. Switched Oscillator With Quarter-Wave, Open-Circuited Stub for Generating Mesoband High-Power Microwave Pulses. *IEEE Trans. Microw. Theory Tech.* **2020**, *68*, 3471–3479. [[CrossRef](#)]
4. Wang, Y.; Chen, D.; Zhang, Z.; Cao, S.; Li, D. A compact wideband high power microwave source based on oil-filled switched oscillator. *High Power Laser Part. Beams* **2019**, *31*, 013002. . [[CrossRef](#)]
5. Rebba Esther Suhasini, D.R.K.; Pandharipande, V.M. Design, development, and performance evaluation of switched wave oscillator (SWO) for high-power electromagnetic applications. *J. Electromagn. Waves Appl.* **2018**, *32*, 1427–1439. [[CrossRef](#)]
6. Achour, Y.; Starzyński, J.; Kasprzycka, W.; Trafny, E.A. Compact low-cost high-voltage pulse generator for biological applications. *Int. J. Circuit Theory Appl.* **2019**, *47*, 1948–1962. [[CrossRef](#)]
7. Santamaria, F.; Echeverri, M.; Roman, F.; Pena, N. Switched Oscillator: Parameter Effects on the Generated Signals. *IEEE Trans. Plasma Sci.* **2012**, *40*, 3433–3441. [[CrossRef](#)]
8. Babaeian, F.; Tyo, J.S.; Fletcher, J.E.; Zhou, H. Cascaded Oscillators for High-Power Microwave Applications. *IEEE Trans. Plasma Sci.* **2023**, *51*, 3111–3122. [[CrossRef](#)]
9. Wu, Z.; Xu, G.; Lu, W.; Ding, E.; Zhang, J. A compact mesoband microwave radiation system. *Rev. Sci. Instrum.* **2022**, *93*, 114707. . [[CrossRef](#)] [[PubMed](#)]
10. Oliveira, L.P.; Vega, F.; Kasmi, C.; AlMansoori, M. Dielectric Resonator Antenna for Compact High-Power Mesoband Generation. In Proceedings of the 2021 IEEE International Symposium on Antennas and Propagation and USNC-URSI Radio Science Meeting (APS/URSI), Singapore, 4–10 December 2021; pp. 1173–1174. [[CrossRef](#)]
11. Jeong, J.; Lee, K.; Ryu, J. High-Q Switched Oscillator With Capacitive Voltage Divider for Generating Mesoband High-Power Microwave Pulses. *IEEE Access* **2021**, *9*, 82325–82334. [[CrossRef](#)]
12. Davidson, D.B. *Computational Electromagnetics for RF and Microwave Engineering*, 2nd ed.; Cambridge University Press: Cambridge, UK, 2011.
13. Chaber, B.; Łodyga, W.; Starzyński, J. Fast electromagnetic field solver for transient antenna simulations. In Proceedings of the 2023 24th International Conference on Computational Problems of Electrical Engineering (CPEE), Grybów, Poland, 10–13 September 2023; pp. 1–4. [[CrossRef](#)]
14. Jin, H. Particle-in-Cell Simulation of Electromagnetic Pulse Generated by High-Power Laser-Target Interaction. Master’s Thesis, Physics, School of Engineering Sciences (SCI), KTH, Stockholm, Sweden, 2018.
15. Hirono, T.; Shibata, Y.; Lui, W.; Seki, S.; Yoshikuni, Y. The second-order condition for the dielectric interface orthogonal to the Yee-lattice axis in the FDTD scheme. *IEEE Microw. Guid. Wave Lett.* **2000**, *10*, 359–361. [[CrossRef](#)]
16. Feizi, M.; Nayyeri, V.; Keshtkar, A. Finite-difference time-domain implementation of tensor impedance boundary conditions. *IET Microw. Antennas Propag.* **2017**, *11*, 1064–1070. . [[CrossRef](#)]
17. Wang, Y.; Wang, J.; Zhang, D. Application of CPML to truncate the open boundaries of cylindrical waveguides in 2.5-dimensional problems. *Sci. China Ser. F Inf. Sci.* **2005**, *48*, 656–669. [[CrossRef](#)]
18. Chaber, B.; Łodyga, W. A Realistic Spark-Gap Model in Computer Simulation of Blumlein Transmission Line. *Energies* **2022**, *15*, 3919. . [[CrossRef](#)]
19. Pouncey, J.C.; Lehr, J.M. A parametric SPICE model for the simulation of spark gap switches. *Rev. Sci. Instrum.* **2020**, *91*, 034704. . [[CrossRef](#)] [[PubMed](#)]
20. Holters, M.; Zolzer, U. A generalized method for the derivation of non-linear state-space models from circuit schematics. In Proceedings of the 2015 23rd European Signal Processing Conference (EUSIPCO), Nice, France, 31 August–4 September 2015. [[CrossRef](#)]
21. Nagel, J. Solving the Generalized Poisson Equation Using the Finite-Difference Method (FDM). 2011. Available online: <https://my.ece.utah.edu/~ece6340/LECTURES/Feb1/Nagel%202012%20-%20Solving%20the%20Generalized%20Poisson%20Equation%20using%20FDM.pdf> (accessed on 1 May 2024).
22. Sandler, S.; King, R. Compact conical antennas for wide-band coverage. *IEEE Trans. Antennas Propag.* **1994**, *42*, 436–439. [[CrossRef](#)]

**Disclaimer/Publisher’s Note:** The statements, opinions and data contained in all publications are solely those of the individual author(s) and contributor(s) and not of MDPI and/or the editor(s). MDPI and/or the editor(s) disclaim responsibility for any injury to people or property resulting from any ideas, methods, instructions or products referred to in the content.